Magnetic order induced by Fe substitution of Al site in the heavy-fermion systems α-YbAlB$_4$ and β-YbAlB$_4$

Kentaro Kuga,[1] Gregory Morrison,[2] LaRico Treadwell,[2] Julia Y. Chan,[2] and Satoru Nakatsuji[1,*]

[1]*Institute for Solid State Physics (ISSP), University of Tokyo, Kashiwa 277-8581, Japan*
[2]*Department of Chemistry, Louisiana State University, Baton Rouge, Louisiana 70803, USA*

β-YbAlB$_4$ is a heavy-fermion superconductor that exhibits a quantum criticality without tuning at zero field and under ambient pressure. We have succeeded in substituting Fe for Al in β-YbAlB$_4$ as well as the polymorphous compound α-YbAlB$_4$, which in contrast has a heavy Fermi-liquid ground state. Full structure determination by single-crystal x-ray diffraction confirmed no change in crystal structure for both α- and β-YbAlB$_4$, in addition to volume contraction with Fe substitution. Our measurements of the magnetization and specific heat indicate that both α-YbAl$_{0.93}$Fe$_{0.07}$B$_4$ and β-YbAl$_{0.94}$Fe$_{0.06}$B$_4$ exhibit a magnetic order, most likely of a canted antiferromagnetic type, at $7 \sim 9$ K. The increase in the entropy as well as the decrease in the antiferromagnetic Weiss temperature with the Fe substitution in both systems indicates that the chemical pressure due to the Fe substitution suppresses the Kondo temperature and induces the magnetism.

$4f$-electron-based heavy-fermion systems have provided prototypical systems to study interesting phenomena in the vicinity of quantum critical points, such as unconventional superconductivity and non-Fermi-liquid states.[1–3] In particular, much attention has been recently paid to unconventional quantum critical materials, such as CeCu$_{6-x}$Au$_x$, YbRh$_2$Si$_2$, and β-YbAlB$_4$,[4–6] which exhibit novel types of quantum criticality beyond the standard spin-density-wave description.[7,8]

The Yb-based heavy-fermion system, YbAlB$_4$, has two polymorphs with different structures: noncentrosymmetric α-YbAlB$_4$ and centrosymmetric β-YbAlB$_4$.[6,9] β-YbAlB$_4$ is the first example of an Yb-based heavy-fermion superconductor with the transition temperature T_c of 80 mK.[6,10] Moreover, it is a unique example of a metal that exhibits a quantum criticality without tuning of any control parameters.[6,11] Strong sensitivity of the non-Fermi-liquid behavior to the magnetic field, in particular, the T/B scaling of the magnetization indicate that the quantum critical point of β-YbAlB$_4$ should be located exactly at zero field under ambient pressure.[11] On the other hand, low-temperature behavior of α-YbAlB$_4$ is well fit to a Fermi-liquid-type description and forms a heavy Fermi-liquid state with the specific heat coefficient $\gamma \sim 130$ mJ/mol K^2 below around $T^* \sim 8$ K.

Up to date, all the $4f$-electron-based quantum critical materials have the valence close to the integer, providing good evidence that these systems can be well described by the Kondo lattice model.[1,3] In sharp contrast, both polymorphs of YbAlB$_4$ are found to be valence fluctuating systems with a strongly intermediate valence, such as Yb$^{2.73+}$ for α-YbAlB$_4$ and Yb$^{2.75+}$ for β-YbAlB$_4$ at 20 K.[12] Strong hybridization has been confirmed by the itinerant f-electron character found in the quantum oscillation study of the Fermi surface of β-YbAlB$_4$.[13]

Interestingly, however, both α- and β-YbAlB$_4$ show Kondo lattice behaviors in the low-energy thermodynamics at low temperatures below the characteristic temperature T^* of 8 K[11,14] and exhibit local moment behavior of Yb^{3+} state in the temperature dependence of the susceptibility and in the electron spin resonance spectra, particularly for the β

phase below T^*.[15] Recent Hall resistivity measurements for β-YbAlB$_4$ revealed a peak at $\sim$40 K, indicating that the coherence appears at a much lower temperature than expected for a strongly intermediate valence state.[16]

In order to understand the origin of the quantum criticality found under ambient condition for β-YbAlB$_4$ as well as the unusual Kondo lattice behavior in the valence fluctuation states found in both α and β phases, it is highly important to reveal the nature of magnetic instability existing nearby the quantum criticality and heavy-fermion state. Here, we report our discovery that Fe substitution for Al site causes antiferromagnetic order in both phases of YbAlB$_4$. Adopting the chemical substitution as a control parameter, we have succeeded in substituting Fe for Al, and discovered that a small Fe substitution of around $5 \sim 7$% is enough to induce an antiferromagnetic order at $7 \sim 9$ K in both α- and β-phases of YbAlB$_4$. Our high-precision determination of the crystal structure indicates no change in the crystal structure by Fe substitution or by temperature sweep at least down to 100 K. The results of the low-temperature susceptibility and specific heat measurements show much stronger temperature dependence than in the pure YbAlB$_4$, indicating that the chemical pressure induced by Fe substitution reduces the Kondo temperature and thereby induces magnetic order.

We have succeeded in growing single crystals of α-YbAl$_{0.93}$Fe$_{0.07}$B$_4$, β-YbAl$_{0.97}$Fe$_{0.03}$B$_4$, β-YbAl$_{0.95}$Fe$_{0.05}$B$_4$, and β-YbAl$_{0.94}$Fe$_{0.06}$B$_4$ using the Al flux growth technique. We have also grown single crystals of a Lu analog, α-LuAl$_{0.79}$Fe$_{0.21}$B$_4$, and β-LuAl$_{0.96}$Fe$_{0.04}$B$_4$. The temperature and field dependence of the magnetization was measured using the commercial SQUID magnetometer (MPMS, Quantum Design). The temperature dependence of the specific heat C_P was measured using a relaxation method. The entropy was estimated by integrating C_P/T over temperature from the lowest temperature 0.4 K of the measurement. The Fe concentration for α-YbAl$_{0.93}$Fe$_{0.07}$B$_4$ was estimated using inductively coupled plasma (ICP) spectroscopy within the resolution of 0.3%, and for β-YbAl$_{1-x}$Fe$_x$B$_4$, α-LuAl$_{0.79}$Fe$_{0.21}$B$_4$, and β-LuAl$_{0.96}$Fe$_{0.04}$B$_4$ by energy-dispersive x-ray analysis (EDX)

TABLE I. Crystallographic data for α-YbAl$_{0.93}$Fe$_{0.07}$B$_4$, β-YbAl$_{0.97}$Fe$_{0.03}$B$_4$, and β-YbAl$_{0.95}$Fe$_{0.05}$B$_4$ at 295(3) and 100(1) K.

Formula	α-**YbAl$_{0.93}$Fe$_{0.07}$B$_4$**		β-**YbAl$_{0.97}$Fe$_{0.03}$B$_4$**		β-**YbAl$_{0.95}$Fe$_{0.05}$B$_4$**	
Temperature (K)	295(3)	100(1)	295(3)	100(1)	295(3)	100(1)
Space group	P*bam*	P*bam*	C*mmm*	C*mmm*	C*mmm*	C*mmm*
a (Å)	5.9184(6)	5.9167(6)	7.3060(9)	7.3010(12)	7.3020(12)	7.3010(12)
b (Å)	11.4645(15)	11.4602(15)	9.3180(12)	9.3130(12)	9.3180(12)	9.3130(12)
c (Å)	3.4832(6)	3.4780(4)	3.4970(3)	3.4890(3)	3.4920(6)	3.4850(6)
V (Å^3)	236.34(6)	235.83(4)	238.07(5)	237.23(5)	237.60(6)	236.96(6)
Z	4	4	4	4	4	4
Crystal dimensions (mm^3)	$0.07 \times 0.13 \times 0.17$		$0.01 \times 0.07 \times 0.07$		$0.01 \times 0.07 \times 0.07$	
Density (g cm^{-3})	6.894	6.904	6.787	6.811	6.801	6.819
θ Range ($^\circ$)	3.55–31.01	3.56–30.97	3.54–30.92	3.54–30.99	3.54–30.96	3.55–30.90
μ (mm^{-1})	39.918	39.972	39.242	39.380	39.320	39.425
Data Collection and Refinement						
Collected reflections	3650	4178	2160	2252	2251	2598
Unique reflections	433	426	244	244	244	243
R_{int}	0.0179	0.0155	0.0133	0.0128	0.0234	0.0203
h	$-8 \leqslant h \leqslant 8$		$-10 \leqslant h \leqslant 10$		$-10 \leqslant h \leqslant 10$	
k	$-16 \leqslant k \leqslant 16$		$-13 \leqslant k \leqslant 13$		$-13 \leqslant k \leqslant 13$	
l	$-5 \leqslant l \leqslant 5$	$-4 \leqslant l \leqslant 5$	$-5 \leqslant l \leqslant 5$		$-4 \leqslant l \leqslant 5$	
$\Delta\rho_{max}$ (e Å^{-3})	3.068	2.999	2.611	2.474	5.223	4.764
$\Delta\rho_{min}$ (e Å^{-3})	-1.862	-1.768	-2.607	-2.758	-4.680	-3.777
GoF	1.149	1.294	1.149	1.159	1.183	1.159
Extinction coefficient	0.0121(10)	0.0119(10)	0.0166(11)	0.0144(10)	0.018(3)	0.014(3)
$^a R_1(F)$ for $F_o^2 > 2\sigma(F_o^2)$	0.0209	0.0237	0.0177	0.0186	0.0388	0.0424
$^b R_w(F_o^2)$	0.0553	0.0603	0.0459	0.0462	0.1016	0.1116

$^a R_1 = \sum ||F_o| - |F_c|| / \sum |F_o|$.

$^b wR_1 = [\sum w(F_o^2 - F_c^2)^2]^{1/2}$; $P = (F_o^2 + 2F_c^2)/3$; $w = 1/[\sigma^2(F_o^2) + (0.0261P)^2 + 3.2341P]$, $w = 1/[\sigma^2(F_o^2) + (0.0258P)^2 + 4.5691P]$, $w = 1/[\sigma^2(F_o^2) + (0.0334P)^2 + 0.8817P]$, $w = 1/[\sigma^2(F_o^2) + (0.0318P)^2 + 2.0681P]$, $w = 1/[\sigma^2(F_o^2) + (0.0852P)^2]$, and $w = 1/[\sigma^2(F_o^2) + (0.0968P)^2]$ for α-YbAl$_{0.93}$Fe$_{0.07}$B$_4$, β-YbAl$_{0.97}$Fe$_{0.03}$B$_4$ and β-YbAl$_{0.95}$Fe$_{0.05}$B$_4$ at 295 K and 100 K, respectively.

within the resolution of 3%. We also utilized the ICP method for some of β-YbAl$_{1-x}$Fe$_x$B$_4$ samples and confirmed the Fe concentration within 1% difference from the EDX results. For example, a single crystal of β-YbAl$_{1-x}$Fe$_x$B$_4$ is found to have $x = 0.03$ by EDX, and $x = 0.02$ by ICP, respectively. Hereafter, we use x(Fe) determined by EDX method for all the samples of β-YbAl$_{1-x}$Fe$_x$B$_4$ and ICP results for α-YbAl$_{1-x}$Fe$_x$B$_4$.

The single-crystal x-ray diffraction experiments were collected using a Nonius Kappa CCD diffractometer equipped with a Mo K$_\alpha$ source ($\lambda = 0.711$ Å) at room temperature, 295(3) K, and at 100(1) K. Direct methods using SIR97[17] was performed to obtain an initial structural model, which was then refined using SHELXL-97.[18] Crystallographic data and atomic coordinates for α-YbAl$_{1-x}$Fe$_x$B$_4$ ($x = 0.07$) and β-YbAl$_{1-x}$Fe$_x$B$_4$ ($x = 0.03, 0.05$) can be found in Tables I–IV. In comparison with the undoped analog, the results clearly show a volume contraction of $\sim 0.8\%$ for α-YbAl$_{0.93}$Fe$_{0.07}$B$_4$, $\sim 0.02\%$ for β-YbAl$_{0.97}$Fe$_{0.03}$B$_4$, and of $\sim 0.2\%$ for β-YbAl$_{0.95}$Fe$_{0.05}$B$_4$, indicating that the Fe doping applies a chemical pressure.

Table II shows the atomic coordinates for α-YbAl$_{1-x}$Fe$_x$B$_4$ ($x = 0.07$). When the Fe substitution was not accounted for, the Al site (4g) had an anomalously small atomic displacement parameter as compared to the undoped α-YbAlB$_4$. Therefore, the Fe was partially substituted on the Al site and the occupancies of the two elements were freely refined. This

resulted in a mixed occupancy of 7.1(15)% Fe and 92.9(15)% Al at 295(3) K and is in good agreement with the composition as obtained from the elemental analysis using the ICP method. Furthermore, no evidence for a structural transition was observed with substitution, and likewise, no structural transition was observed for any Fe concentration upon cooling from room temperature down to 100(1) K.

Tables III and IV provide atomic coordinates for β-YbAl$_{1-x}$Fe$_x$B$_4$ ($x = 0.03, 0.05$). When the Fe substitution was not included in the model, the Al site (4g) had a similar atomic displacement parameter to the Yb site (4i) suggesting that the Fe occupies the Al site. For β-YbAl$_{0.97}$Fe$_{0.03}$B$_4$, Fe was partially substituted onto the Al site and the occupancies were freely refined. The resulting site occupancy was 1.3(15)% Fe and 98.7(15)% Al at 295(3) K. This is in agreement with the ICP data which indicated the stoichiometry to be β-YbAl$_{0.98}$Fe$_{0.02}$B$_4$. While the atomic displacement parameters also suggested that the Fe occupied the Al site in β-YbAl$_{0.95}$Fe$_{0.05}$B$_4$, no Fe could be refined onto this site, or any other site, for the model. The inability to model the Fe doping in β-YbAl$_{0.95}$Fe$_{0.05}$B$_4$ can be attributed to the lower-quality diffraction data for this analog compared to the other analogues. β-YbAl$_{0.95}$Fe$_{0.05}$B$_4$ grew as thin plates whereas β-YbAl$_{0.97}$Fe$_{0.03}$B$_4$ grew as thick plates and α-YbAl$_{0.93}$Fe$_{0.07}$B$_4$ grew as rods. The thinner plates for β-YbAl$_{0.95}$Fe$_{0.05}$B$_4$ led to lower-quality x-ray diffraction data, which is apparent in both the increased R$_1$ and residual electron densities for this

TABLE II. Atomic coordinates and displacement parameters for α-Yb$_1$Al$_{1-x}$Fe$_x$B$_4$($x = 0.07$) at 295(3) and 100(1) K.

Atom	Wyckoff site	x	y	z	U_{eq} (Å^2)[a]	Occ.
295(3) K						
Yb1	4g	0.12859(5)	0.15052(3)	0	0.00344(17)	1
Al1	4g	0.1365(4)	0.4109(2)	0	0.0042(8)	0.929(15)
Fe1	4g	0.1365(4)	0.4109(2)	0	0.0042(8)	0.071(15)
B1	4h	0.2921(16)	0.3135(8)	1/2	0.0056(16)	1
B2	4h	0.3654(15)	0.4695(8)	1/2	0.0054(16)	1
B3	4h	0.3850(16)	0.0479(8)	1/2	0.0063(15)	1
B4	4h	0.4725(16)	0.1939(8)	1/2	0.0042(16)	1
100(1) K						
Yb1	4g	0.12862(6)	0.15052(3)	0	0.00166(19)	1
Al1	4g	0.1361(4)	0.4109(2)	0	0.0023(9)	0.935(17)
Fe1	4g	0.1361(4)	0.4109(2)	0	0.0023(9)	0.065(17)
B1	4h	0.2915(19)	0.3138(9)	1/2	0.0047(18)	1
B2	4h	0.3651(17)	0.4686(8)	1/2	0.0032(17)	1
B3	4h	0.3875(17)	0.0482(9)	1/2	0.0023(16)	1
B4	4h	0.4751(18)	0.1929(9)	1/2	0.0037(18)	1

[a]U_{eq} is defined as one third of the trace of the orthogonalized U_{ij} tensor.

analog. Due to the increased $\Delta\rho_{min/max}$, the Fe substitution could not be modeled. As with α-YbAl$_{1-x}$Fe$_x$B$_4$, no structural transition was observed in β-YbAl$_{1-x}$Fe$_x$B$_4$ upon doping or cooling from 298 K down to 100 K.

Single-crystal x-ray diffraction data was also collected on a sample of β-YbAl$_{1-x}$Fe$_x$B$_4$($x = 0.06$). Although the mosaicity of the single crystal was suitable for data collection at 295(3) K, upon cooling in 50 K intervals down to 100(1) K, a continuous decrease in crystal quality, indicated by increased χ^2s and mosaicity, was observed. For example, the mosaicity of the crystal increased from 0.45 degrees at 295(3) K to 0.87 degrees at 100(1) K. When the crystal was warmed back to room temperature, the crystal quality returned to its original state. Diffraction data of β-YbAl$_{1-x}$Fe$_x$B$_4$($x = 0.06$) was collected at both 295(3) K and 100(1) K and no evidence for a structural transition was observed. In α-YbAl$_{1-x}$Fe$_x$B$_4$ ($x = 0.07$) and β-YbAl$_{1-x}$Fe$_x$B$_4$($x = 0.03, 0.05$), on the other hand, the degradation of crystal quality on cooling was not observed. Our synthesis experiments suggest that the concentration $x = 0.06$ is close to the edge of the stability of the Fe doped β-phase, and this may be the origin of the increase in the mosaicity on cooling. The cause of this decrease

TABLE III. Atomic coordinates and displacement parameters for β-YbAl$_{1-x}$Fe$_x$B$_4$($x = 0.03$[a]) at 295(3) and 100(1) K.

Atom	Wyckoff site	x	y	z	U_{eq} (Å^2)[b]	Occ.
295(3) K						
Yb1	4i	0	0.30065(3)	0	0.00388(19)	1
Al1	4g	0.1808(3)	0	0	0.0042(8)	0.987(15)
Fe1	4g	0.1808(3)	0	0	0.0042(8)	0.013(15)
B1	4h	0.1219(13)	1/2	1/2	0.0050(13)	1
B2	8q	0.2226(8)	0.1594(14)	1/2	0.0061(10)	1
B3	4j	0	0.0922(9)	1/2	0.0044(13)	1
100(1) K						
Yb1	4i	0	0.30066(3)	0	0.00260(19)	1
Al1	4g	0.1810(3)	0	0	0.0031(8)	0.996(15)
Fe1	4g	0.1810(3)	0	0	0.0031(8)	0.004(15)
B1	4h	0.1215(13)	1/2	1/2	0.0046(14)	1
B2	8q	0.2224(8)	0.1596(8)	1/2	0.0046(10)	1
B3	4j	0	0.0921(9)	1/2	0.0043(14)	1

[a]$x = 0.03(2)$ is estimated by EDX method, while ICP yields $x = 0.02(1)$ with better accuracy, close to the above Fe occupancy obtained from the structural analysis.
[b]U_{eq} is defined as one-third of the trace of the orthogonalized U_{ij} tensor.

TABLE IV. Atomic Coordinates and Displacement Parameters for β-YbAl$_{1-x}$Fe$_x$B$_4$ ($x = 0.05$) at 295(3) and 100(1) K

Atom	Wyckoff site	x	y	z	U_{eq} (Å^2)[a]	Occ.
295(3) K						
Yb1	$4i$	0	0.30070(4)	0	0.0054(4)	1
Al1	$4g$	0.1799(6)	0	0	0.0049(8)	1
B1	$4h$	0.122(3)	1/2	1/2	0.005(2)	1
B2	$8q$	0.2225(12)	0.1607(15)	1/2	0.0067(17)	1
B3	$4j$	0	0.0917(15)	1/2	0.006(2)	1
100(1) K						
Yb1	$4i$	0	0.30072(5)	0	0.0042(4)	1
Al1	$4g$	0.1802(6)	0	0	0.0031(8)	1
B1	$4h$	0.124(3)	1/2	1/2	0.009(3)	1
B2	$8q$	0.2227(15)	0.1598(18)	1/2	0.009(2)	1
B3	$4j$	0	0.0913(12)	1/2	0.004(3)	1

[a]U_{eq} is defined as one-third of the trace of the orthogonalized U_{ij} tensor.

in crystal quality is currently being explored and will be the subject of a future manuscript.

Figures 1(a) and 1(b) show the temperature dependence of the susceptibility $\chi = M/H$ for both α-YbAl$_{1-x}$Fe$_x$B$_4$ and β-YbAl$_{1-x}$Fe$_x$B$_4$, respectively. The susceptibility for both systems is clearly Ising-like. Namely, the c-axis susceptibility is strongly temperature dependent, while the ab-plane component is nearly temperature independent with a small value of ~ 0.005 emu/mol. The c-axis component for α-YbAlB$_4$ exhibits no anomaly down to 2 K, and start leveling off below $T^* = 8$ K, indicating the onset of the Fermi-liquid ground state.[11,14] In contrast, the c-axis susceptibility for β-YbAlB$_4$ exhibits divergent behavior on cooling, reflecting the unconventional quantum criticality.[6,11] With doping of Fe by 3%, the c-axis susceptibility for β-YbAl$_{0.97}$Fe$_{0.03}$B$_4$

exhibits a weaker temperature dependence with a smaller value than the pure case below ~ 20 K, while it completely overlaps that for the pure β-YbAlB$_4$ at $T > 20$ K. In contrast, no change was found in the ab-plane component by doping of Fe by 3% for the β phase [Fig. 1(b)].

With further substitution of Fe at the Al site, however, both α-YbAl$_{0.93}$Fe$_{0.07}$B$_4$ and β-YbAl$_{0.94}$Fe$_{0.06}$B$_4$ exhibit a weak kink in the temperature dependence of the c-axis susceptibility at 7.5(5) K and 9.5(5) K, respectively and bifurcate into different curves for zero-field-cooled and field-cooled sequences. More clear anomaly and hysteresis was found in the temperature dependence of the ab-plane susceptibility, suggesting the ferromagnetic component lies in the ab plane. The insets of Figs. 1(a) and 1(b) show the field dependence of the magnetization of α-YbAl$_{0.93}$Fe$_{0.07}$B$_4$
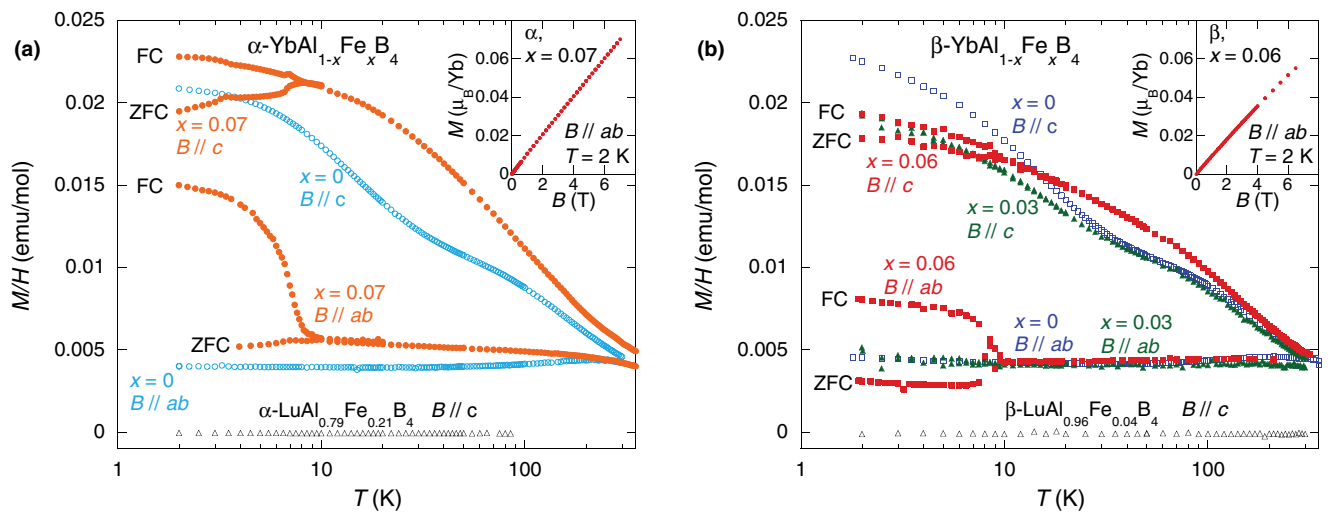

FIG. 1. (Color online) (a) Temperature dependence of the ab-plane and c-axis susceptibility of α-YbAlB$_4$ (open circle), α-YbAl$_{0.93}$Fe$_{0.07}$B$_4$ (closed circle) measured under a field of 10 mT, and of α-LuAl$_{0.79}$Fe$_{0.21}$B$_4$ (open triangle) under 1 T. (b) Temperature dependence of the ab-plane and c-axis susceptibility of β-YbAlB$_4$ (open square), β-YbAl$_{0.97}$Fe$_{0.03}$B$_4$ (closed triangle) and β-YbAl$_{0.94}$Fe$_{0.06}$B$_4$ (closed square) measured under a field of 10 mT, and of β-LuAl$_{0.96}$Fe$_{0.04}$B$_4$ under 1 T. For all measurements, both zero-field-cooling and field-cooling sequences are employed. The inset of each panel shows the magnetic field dependence of the magnetization M of α-YbAl$_{0.93}$Fe$_{0.07}$B$_4$ and β-YbAl$_{0.94}$Fe$_{0.06}$B$_4$ under a field up to 7 T along the ab plane at 2 K.
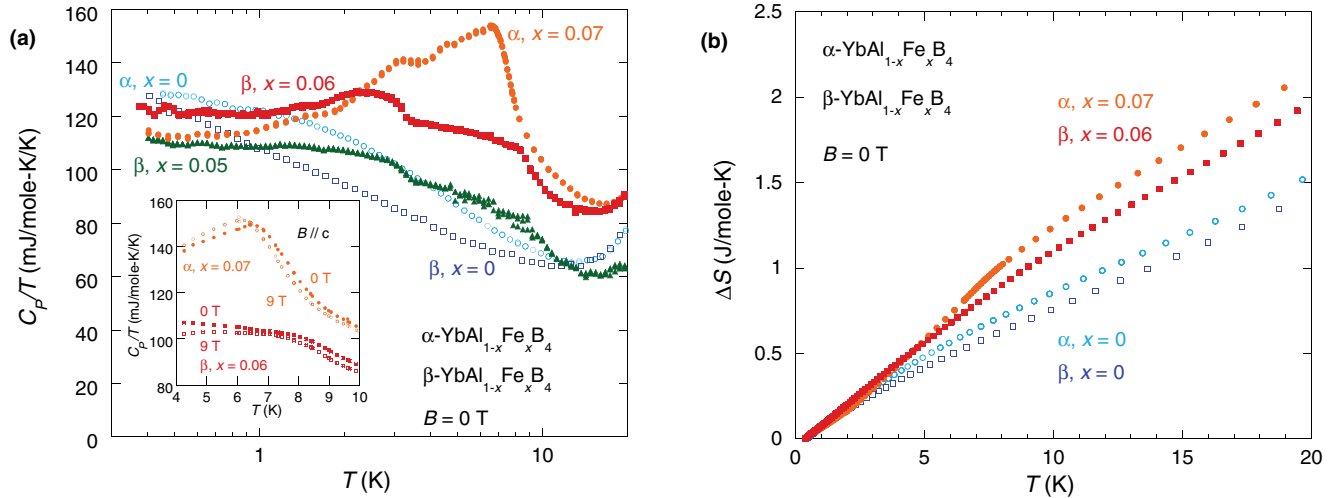
FIG. 2. (Color online) Temperature dependence of (a) the specific heat divided by temperature C_P/T and (b) the entropy of α-YbAlB$_4$ (open circle), α-YbAl$_{0.93}$Fe$_{0.07}$B$_4$ (closed circle), β-YbAlB$_4$ (open square), β-YbAl$_{0.94}$Fe$_{0.06}$B$_4$ (closed square), and β-YbAl$_{0.95}$Fe$_{0.05}$B$_4$ (closed triangle). The panel (a) inset is the temperature dependence of C_P/T near the transition temperature under 0 T (closed circle for α-YbAl$_{0.93}$Fe$_{0.07}$B$_4$ and closed square for β-YbAl$_{0.94}$Fe$_{0.06}$B$_4$) and 9 T (open circle for α-YbAl$_{0.93}$Fe$_{0.07}$B$_4$ and open square for β-YbAl$_{0.94}$Fe$_{0.06}$B$_4$) along the c axis.

and β-YbAl$_{0.94}$Fe$_{0.06}$B$_4$ under a field along ab plane at 2 K. For each measurement, the sample was first cooled down to 2 K from the paramagnetic state under zero field. Then, the field was increased up to 7 T and decreased back to zero to obtain a magnetization curve. Each sample shows an almost linear magnetic field dependence of the magnetization and no hysteresis was found within experimental resolution of $1 \times 10^{-4} \mu_B$/Yb, which places the upper bound for the ferromagnetic component along the ab plane. Both linear magnetization curve and the small size of the spontaneous moment point to a canted antiferromagnetism. On the other hand, the temperature dependence of the susceptibility for the Lu analog α-LuAl$_{0.79}$Fe$_{0.21}$B$_4$ and α-LuAl$_{0.96}$Fe$_{0.04}$B$_4$ shown in Figs. 1(a) and (b) shows diamagnetism with a small negative value in between -1×10^{-4} to -3×10^{-5} emu/mol, indicating that Fe ion is nonmagnetic and thus it is $4f$ moments of Yb ion that form the magnetic order in both α-YbAl$_{0.93}$Fe$_{0.07}$B$_4$ and β-YbAl$_{0.94}$Fe$_{0.06}$B$_4$.

Figure 2 presents the temperature dependence of the specific heat divided by temperature C_P/T at 0 T. Both pure phases show paramagnetic behavior down to the lowest temperatures. Namely, C_P/T for α-YbAlB$_4$ gradually increases on cooling and saturates to a large value of around 130 mJ/mol K^2, indicating the formation of a heavy Fermi-liquid state.[11,14] C_P/T for β-YbAlB$_4$ shows a logarithmic divergence, consistent with the non-Fermi-liquid ground state.[6,11]

On the other hand, the doping of Fe induces the anomalies in C_P/T due to the magnetic transitions: α-YbAl$_{0.93}$Fe$_{0.07}$B$_4$ exhibits a peak at 6.7(3) K and β-YbAl$_{0.95}$Fe$_{0.05}$B$_4$ and β-YbAl$_{0.94}$Fe$_{0.06}$B$_4$ show a shoulderlike anomaly at 8.3 K. Given the tails of the anomalies with a temperature width of ~ 1 K, these confirm the bulk nature of the magnetic transition inferred from the above susceptibility measurements. The inset of Fig. 2 presents the temperature dependence of C_P/T under fields of 0 T and 9 T along the c axis. The application of a magnetic field of 9 T slightly decreases the peak temperature

of C_P/T by ~ 0.5 K, indicating that the magnetic ordered state is not ferromagnetic but antiferromagnetic. On further cooling, all the doped samples show an additional anomaly at around 3 K, suggesting another magnetic transition, which is not seen in the temperature dependence of the susceptibility. For β-YbAl$_{1-x}$Fe$_x$B$_4$, the fact that both low- and high-temperature anomalies appear at nearly the same temperatures for both $x = 0.05$ and 0.06 indicates that both transitions are intrinsic and not due to the mosaicity found for $x = 0.06$. One possible origin of the low-temperature anomaly is the change of the magnetic structure. Further microscopic studies such as neutron diffraction and nuclear magnetic resonance measurements are necessary to determine the spin structure.

In order to gain the insight of the origin of the magnetic order induced by Fe substitution, we made the Curie-Weiss (CW) analysis for the susceptibility. For both pure α- and β-phases as well as β-YbAl$_{0.97}$Fe$_{0.03}$B$_4$, the susceptibility above 20 K collapses on top of each other and the CW fitting at $T > 150$ K yields the effective moment P_{eff} of 2.2(2) μ_B and the antiferromagnetic (AFM) Weiss temperature Θ_W of 110(5) K.[11,14] On the other hand, the same fitting at $T > 150$ K for α-YbAl$_{0.93}$Fe$_{0.07}$B$_4$ and β-YbAl$_{0.94}$Fe$_{0.06}$B$_4$ respectively yields $P_{\mathrm{eff}} = 2.44$ μ_B and AFM $\Theta_W = 60$ K, and $P_{\mathrm{eff}} = 2.2(2)$ μ_B and AFM $\Theta_W = 80$ K. The analyses indicate that the Fe substitution reduces the Weiss temperature by $30 \sim 40$%. This suggests that the Kondo temperature, which is estimated to be ~ 200 K for both pure α and β phases,[6,11,14] becomes significantly suppressed by Fe doping. This is consistent with the chemical pressure effect inferred from the crystal structure analysis, as the pressure normally renders the Yb system more magnetic.

Correspondingly, the entropy for both phases estimated by integrating C_P/T from the lowest $T = 0.4$ K [Fig. 2(b)] indicates a substantial increase at 20 K with the Fe substitution of $6 \sim 7$%. In both pure systems, the ground state of the crystal electric field scheme is known to have a Kramers doublet,

which is most likely separated by more than 100 K from the exited doublet state.[14,19] Assuming that the gap scale stays the same by Fe doping, we may conclude that the increase of the entropy at 20 K indicates again the suppression of the Kondo temperature. Moreover, even at the magnetic transition temperatures $\sim$9 K, the entropy of both α-YbAl$_{0.93}$Fe$_{0.07}$B$_4$ and β-YbAl$_{0.94}$Fe$_{0.06}$B$_4$ is larger than the pure systems by $\sim$0.3 mJ/mol-K. This value is too large for a pure ferromagnetic transition given the spontaneous moment $< 0.001 \mu_B$/Yb estimated by the magnetization measurement. This also provides another evidence that the observed hysteresis is due to a canted antiferromagnetism, not by a simple ferromagnetism.

To summarize, we found that the Fe substitution at Al site induces a magnetic order, most likely a canted antiferromagnetic type due to $4f$ electrons, by suppressing the Kondo temperature. The crystal structure analysis indicates that the Fe substitution decreases the volume without having any structural transition. Combined, the magnetic order is induced in both α-YbAlB$_4$ and β-YbAlB$_4$ because of the chemical pressure applied by the Fe substitution and thus indicates the proximity to a magnetic instability for both phases of YbAlB$_4$ at ambient pressure. The detailed study for the ground state evolution from pure α- and β-YbAlB$_4$ with more fine steps of Fe doping is necessary to clarify how a magnetic quantum criticality emerges and develops with doping Fe in both α- and β-phases. It is also an interesting future issue how a putative magnetic quantum criticality induced by the Fe substitution is related with the unconventional quantum criticality observed in the heavy-fermion superconductor β-YbAlB$_4$.

---

*satoru@issp.u-tokyo.ac.jp

[1] H. V. Löhneysen, A. Rosch, M. Vojta, and P. Wölfle, Rev. Mod. Phys. **79**, 1015 (2007).

[2] P. Monthoux, D. Pines, and G. G. Lonzarich, Nature (London) **450**, 1177 (2007).

[3] P. Gegenwart, Q. Si, and F. Steglich, Nature Phys. **4**, 186 (2008).

[4] H. V. Lohneysen, T. Pietrus, G. Portisch, H. G. Schlager, A. Schroder, M. Sieck, and T. Trappmann, Phys. Rev. Lett. **72**, 3262 (1994).

[5] O. Trovarelli, C. Geibel, S. Mederle, C. Langhammer, F. M. Grosche, P. Gegenwart, M. Lang, G. Sparn, and F. Steglich, Phys. Rev. Lett. **85**, 626 (2000).

[6] S. Nakatsuji, K. Kuga, Y. Machida, T. Tayama, T. Sakakibara, Y. Karaki, H. Ishimoto, S. Yonezawa, Y. Maeno, E. Pearson, G. G. Lonzarich, L. Balicas, H. Lee, and Z. Fisk, Nature Phys. **4**, 603 (2008).

[7] T. Moriya, *Spin Fluctuations in Itinerant Electron Magnetism* (Springer, Berlin, 1985).

[8] A. J. Millis, Phys. Rev. B **48**, 7183 (1993).

[9] R. T. Macaluso, S. Nakatsuji, K. Kuga, E. L. Thomas, Y. Machida, Y. Maeno, Z. Fisk, and J. Y. Chan, Chem. Mater. **19**, 1918 (2007).

[10] K. Kuga, Y. Karaki, Y. Matsumoto, Y. Machida, and S. Nakatsuji, Phys. Rev. Lett. **101**, 137004 (2008).

[11] Y. Matsumoto, S. Nakatsuji, K. Kuga, Y. Karaki, N. Horie, Y. Shimura, T. Sakakibara, A. H. Nevidomskyy, and P. Coleman, Science **21**, 316 (2011).

[12] M. Okawa, M. Matsunami, K. Ishizaka, R. Eguchi, M. Taguchi, A. Chainani, Y. Takata, M. Yabashi, K. Tamasaku, Y. Nishino, T. Ishikawa, K. Kuga, N. Horie, S. Nakatsuji, and S. Shin, Phys. Rev. Lett. **104**, 247201 (2010).

[13] E. C. T. O'Farrell, D. A. Tompsett, S. E. Sebastian, N. Harrison, C. Capan, L. Balicas, K. Kuga, A. Matsuo, K. Kindo, M. Tokunaga, S. Nakatsuji, G. Csányi, Z. Fisk, and M. L. Sutherland, Phys. Rev. Lett. **102**, 216402 (2009).

[14] Y. Matsumoto, K. Kuga, T. Tomita, Y. Karaki, and S. Nakatsuji, Phys. Rev. B **84**, 125126 (2011).

[15] L. M. Holanda, J. M. Vargas, W. Iwamoto, C. Rettori, S. Nakatsuji, K. Kuga, Z. Fisk, S. B. Oseroff, and P. G. Pagliuso, Phys. Rev. Lett. **107**, 026402 (2011).

[16] E. C. T. O'Farrell, Y. Matsumoto, and S. Nakatsuji, Phys. Rev. Lett. **109**, 176405 (2012).

[17] A. Altomare, M. C. Burla, M. Camalli, G. L. Cascarano, C. Giacovazzo, A. Guagliardi, A. G. G. Moliterni, G. Polidori, and R. Spagna, J. Appl. Crystallogr. **32**, 115 (1999).

[18] G. M. Sheldrick, Acta Crystallogr. Sect. A **64**, 112 (2008).

[19] A. H. Nevidomskyy and P. Coleman, Phys. Rev. Lett. **102**, 077202 (2009).